

Article

Further Insight into the Manganese(II) 2,2'-Bipyridine-1,1'-dioxide Homoleptic Complex: Single-Crystal X-ray Structure Determination of the Perchlorate Salt and DFT Calculations

Jesús Castro ¹, Valentina Ferraro ²  and Marco Bortoluzzi ^{2,3,*} 

¹ Departamento de Química Inorgánica, Facultad de Química, Universidade de Vigo, Edificio de Ciencias Experimentais, 36310 Vigo, Galicia, Spain; jesusca@uvigo.gal

² Dipartimento di Scienze Molecolari e Nanosistemi, Università Ca' Foscari Venezia, 30172 Mestre, Italy

³ CIRCC, via Celso Ulpiani 27, 70126 Bari, Italy

* Correspondence: markos@unive.it; Tel.: +39-0412348651

Abstract: The homoleptic cationic complex formed by reacting suitable manganese(II) salts with 2,2'-bipyridine-1,1'-dioxide (bipyO₂) has been subjected to several studies in the past because of its peculiar absorption and electrochemical features. Here, the first single-crystal X-ray structure determination of a [Mn(bipyO₂)₃]²⁺ salt is reported, where the charge of the cation is balanced by perchlorate anions. The hydrated salt [Mn(bipyO₂)₃](ClO₄)₂ crystallizes in the monoclinic system (P2₁/n space group) and the asymmetric unit contains three cationic complexes and six perchlorate anions. The environment of the manganese(II) ions is best described as octahedral, with scarce variations among the three cations in the asymmetric unit. The bipyO₂ ligands exhibit κ² coordination mode, forming seven-membered metallacycles. The X-ray outcomes have been used as the starting point for DFT and TDDFT calculations, aimed to elucidate the charge transfer origin of the noticeable absorption in the visible range. The MLCT nature is confirmed by the hole and electron distributions associated with the spin-allowed transitions. DFT calculations on the related manganese(III) complex indicate that the geometry of [Mn(bipyO₂)₃]²⁺ changes only slightly upon oxidation, in agreement with the reversible electrochemical behaviour experimentally observed.

Keywords: manganese(II); bipyridine dioxide; single-crystal X-ray diffraction; DFT calculations; absorption spectroscopy; cyclic voltammetry



Citation: Castro, J.; Ferraro, V.; Bortoluzzi, M. Further Insight into the Manganese(II) 2,2'-Bipyridine-1,1'-dioxide Homoleptic Complex: Single-Crystal X-ray Structure Determination of the Perchlorate Salt and DFT Calculations. *Crystals* **2024**, *14*, 422. <https://doi.org/10.3390/cryst14050422>

Academic Editor: Vladimir P. Fedin

Received: 19 April 2024

Revised: 26 April 2024

Accepted: 27 April 2024

Published: 29 April 2024



Copyright: © 2024 by the authors. Licensee MDPI, Basel, Switzerland. This article is an open access article distributed under the terms and conditions of the Creative Commons Attribution (CC BY) license (<https://creativecommons.org/licenses/by/4.0/>).

1. Introduction

The adoption of 2,2'-bipyridine-1,1'-dioxide (bipyO₂) as a ligand in coordination chemistry began in the 1960s, with the preparation of complexes of some divalent and trivalent metal ions belonging to the first-row transition series and to Group 12 [1–3]. The homoleptic manganese(II) complex [Mn(bipyO₂)₃]²⁺ was obtained either as perchlorate or as tetrachloro-platinate salt, and characterized through elemental analysis, conductivity and magnetic measurements, and IR spectroscopy. The formulae indicate that bipyO₂ acts as a bidentate O-donor, forming a seven-membered metallacycle upon coordination. The related manganese(III) complex was synthesized using potassium persulphate as oxidant and isolated as perchlorate or persulphate salt. Halide salts of the manganese(II) complex with the general formula [Mn(bipyO₂)₃]X₂ (X = Br, I) were obtained in 1964 using the corresponding hydrated metal halides as reactants. The characterization data were corroborated with the collection of the absorption spectra in DMF solutions. The orange color, associated with absorptions in the visible range with a maximum at 410 nm, was attributed to charge transfer transitions [4]. The replacement of the metal precursor with manganese(II) chloride or thiocyanate afforded different complexes. In particular, a polymeric derivative with bridging chloro-ligands was proposed as the product of the reaction between bipyO₂ and

MnCl₂ in ethanol, while the characterization data suggested the formation of the mononuclear heteroleptic complex [Mn(*N*-NCS)₂(bipyO₂)₂] starting from Mn(NCS)₂. In both cases, an octahedral environment was expected around manganese(II) [5].

In subsequent studies, an absorption band centred at 428 nm was assigned to charge transfer processes in the [Mn(bipyO₂)₃]²⁺ cation [6]. The population of the corresponding excited state appears to cause the destabilization of the complex, with consequent progressive decomposition [7]. The same phenomenon was observed also for related pyridine-*N*-oxide and quinoline-*N*-oxide homoleptic manganese(II) complexes [8]. The depopulation of the excited states does not seem to follow radiative decay routes, since no study concerning the photoluminescence of [Mn(bipyO₂)₃]²⁺ has ever been reported. The absorption and emission features are completely different compared to those exhibited by homoleptic manganese(II) complexes with bidentate phosphine oxides in the coordination sphere [9–11]. In the absorption spectra of these last compounds, no band attributable to charge transfer processes is present, while the emission spectra show bands associated with the ⁴T₁(⁴G) → ⁶A₁(⁶S) metal-centred transition.

EPR data concerning the [Mn(bipyO₂)₃]²⁺ cation were also reported and, based on the splitting parameter *A* (92 G), it was concluded that the metal–ligand bonds have a covalent character comparable to those in [Mn(NCCH₃)₆]²⁺ and [Mn(H₂O)₆]²⁺, but lower compared to the related homoleptic 2,2′-bipyridine complex. Electrochemical measurements on acetonitrile solutions revealed that the complex is oxidized in two reversible one-electron steps at E_{1/2} = 0.87 V and 1.62 V vs. SCE [6]. The ease of oxidation of manganese(II) once surrounded by bipyO₂ is another element of difference in comparison with the bidentate phosphine oxide derivatives. Thanks to these redox properties, the manganese(III) complex [Mn(bipyO₂)₃]³⁺ was used in a kinetic study as oxidant towards the copper(I) complex [Cu(dmp)₂]⁺ (dmp = 2,9-dimethyl-1,10-phenanthroline) [12].

Despite the presence in the literature of several characterization data, the [Mn(bipyO₂)₃]²⁺ complex was never structurally investigated. Moreover, the electronic structure of the complex, at the basis of the absorption features and the redox properties, was never studied from a computational point of view. Here, we report the single-crystal X-ray structure determination of the hydrated perchlorate salt of [Mn(bipyO₂)₃]²⁺, representing a rare example of structural characterization of a homoleptic bipyO₂ metal complex. The X-ray outcomes have been used as starting point for DFT and TDDFT calculations, aimed to elucidate the absorption and electrochemical features of the complex.

2. Experimental Section

2.1. Materials and Methods

Manganese(II) perchlorate hexahydrate, lithium perchlorate, 2,2′-bipyridine, 30% hydrogen peroxide water solution, ferrocene (Fc) and organic solvents were purchased from Merck (Darmstadt, Germany). All the reactants were used as received, except for acetonitrile, which was purified before use according to established methods [13]. In addition, 2,2′-bipyridine-1,1′-dioxide (bipyO₂) was synthesized following a reported procedure [1]. In a typical preparation, a solution containing 5000 g of 2,2′-bipyridine (32.0 mmol) in 40 mL of glacial acetic acid and 6 mL of 30% hydrogen peroxide water solution was heated at 70 °C for 3 h. Further hydrogen peroxide solution (4.5 mL) was then added to the reaction mixture, which was kept under stirring at 70 °C for 20 h. After cooling at room temperature, acetone was added until the precipitation of a solid occurred, which was then filtered. The crude product was dissolved in the minimal volume of hot water. After cooling, acetone was slowly added until the complete precipitation of the white solid, which was collected by filtration, washed two times with 15 mL of acetone, and dried under vacuum. Yield: 90% (5.425 g). Characterization data are in agreement with those recently reported for the same compound obtained with a different synthetic approach [14]. [Mn(bipyO₂)₃](ClO₄)₂·2H₂O was synthesized based on reported procedures [1,4]. Mn(ClO₄)₂·6H₂O (0.362 g, 1.0 mmol) was dissolved in about 2 mL of distilled water at room temperature. A solution containing 3.2 mmol (0.602 g) of bipyO₂ dissolved in the minimum volume of water (about 10 mL)

was slowly added. After a few minutes, the product started to separate as an orange solid. The reaction mixture was kept under stirring at room temperature for three hours and then cooled with an ice bath. After twenty minutes the solid was filtered, washed twice with 5 mL of ethanol, and dried under vacuum. Yield: 80% (0.524 g). Selected characterization data are reported in the Section 3. Crystals suitable for X-ray diffraction were collected from the slow evaporation of water solutions.

Carbon, hydrogen and nitrogen elemental analyses were obtained using an Elementar (Langensfeld, Germany) Unicube microanalyzer. Magnetic susceptibility measurements were carried out on solid samples at 298 K and 3.5 kGauss magnetic field strength using an MK1 magnetic susceptibility balance (Sherwood Scientific Ltd., Cambridge, UK). The measured magnetic susceptibility was corrected for the diamagnetic contribution using tabulated Pascal's constants [15]. IR spectra in KBr (spectroscopy grade, Merck) were collected in the 4000–450 cm^{-1} range using a Perkin-Elmer (Shelton, CT, USA) SpectrumOne spectrophotometer. ^1H NMR spectra were collected in D_2O (Eurisotop, Saint-Aubin, France) employing a Bruker Avance 400 instrument (Billerica, MA, USA) operating at 400.13 MHz of ^1H resonance. Spectra were referred to the partially non-deuterated fraction of the solvent, itself quoted to sodium trimethyl-silyl-propane-sulfonate. Conductivity measurements in acetone were carried out with a Radiometer (Copenhagen, Denmark) CDM83 instrument and compared with literature data [16]. Cyclic voltammetry measurements in acetonitrile containing 0.1 M LiClO_4 were conducted using an eDAQ (Denistone, Australia) ET014-199 instrument coupled with an eDAQ ET074-1 glassy carbon working electrode (1 mm diameter) and an eDAQ ET078-1 Pt-coated titanium rod auxiliary electrode. All the measurements were carried out under argon at room temperature. Ferrocene was introduced as internal standard and a Pt wire was used as pseudo-reference electrode. CV data are reported following the IUPAC convention [17]. Absorption spectra in dichloromethane at room temperature were recorded in a 10×10 mm fluorescence quartz cuvette (Hellma GmbH, Müllheim, Germany) with an OceanOptics (Ocean Insight, Orlando, FL, USA) HR4000CG UV-NIR detector, fiber-coupled to an OceanOptics CUV-ALL-UV cuvette holder equipped with collimators and an OceanOptics FHS-UV in-line filter holder. The cuvette holder was fiber-coupled to an OceanOptics DH-2000-BAL deuterium-halogen lamp. The angle between the source and the detector was 180° . The experimental equipment was further coupled with an OceanOptics LSM-405A LED light source centred at 405 nm for photodecomposition studies (output power 10 mW), or with OceanOptics LSM-310A and LSM-365A UV LED light sources for emission measurements. The angle between the LED sources and the detector was 90° . Attempts to investigate possible luminescence of solid samples at room temperature were carried out using a Horiba Jobin Yvon (Kyoto, Japan) Fluorolog-3 spectrofluorometer, equipped with a continuous-wave xenon arc lamp coupled to a double Czerny–Turner monochromator as excitation source and a single grating monochromator coupled to a Hamamatsu (Shizuoka, Japan) R928 photomultiplier tube as detection system.

2.2. Crystal Structure Determination

Crystallographic data were collected at CACTI (Universidade de Vigo) using a Bruker (Billerica, MA, USA) D8 Venture Photon II CMOS detector and $\text{Mo-K}\alpha$ radiation ($\lambda = 0.71073 \text{ \AA}$) generated by an Incoatec (Geesthacht, Germany) Microfocus Source $\text{I}\mu\text{S}$. The temperature was maintained at 100 K during the acquisition employing an Oxford Cryosystems (Oxford, UK) Cryostream 800 cooler. The software APEX4 v.2022.1-1 was used for collecting frames of data, indexing reflections, and the determination of lattice parameters [18]. The integration of the intensity of reflections was carried out with SAINT version 8.40B, and SADABS version 2016/2 was used for scaling and empirical absorption correction [18]. The crystallographic treatment was performed with the Oscale program version 4.7.1 [19] and solved using the SHELXT version 2018/2 program [20]. The structure was subsequently refined by a full-matrix least-squares based on F^2 using the SHELXL version 2019/2 program [21]. Non-hydrogen atoms were refined with anisotropic displacement parameters. Hydrogen atoms were included in idealized positions and refined with

isotropic displacement parameters. The asymmetric unit is formed by three dicationic coordination compounds, six monoanionic molecules and an undetermined number of water molecules, of which only three were modelled. A fourth oxygen atom (another water molecule) and high residual density were not modelled further. In addition, some oxygen atoms belonging to perchlorate anions maintain high thermal ellipsoids, probably because they are split over two positions, but the disorder was not modelled. Any attempt to obtain another higher symmetry was unsuccessful, and no symmetry operation was found between the three components. For this reason, we decided to study another monocrystal from a repeated synthesis, but the results obtained were comparable, since again three cations and six anions were present in the asymmetric unit. Some water molecules (oxygen atoms) were also found in the asymmetric unit, although the corresponding hydrogen atoms were not modelled this time. CCDC 2260009 and 2260010 contain the supplementary crystallographic data for the crystals studied. Since the two crystalline compounds are quite similar, in the discussion only the first is considered. Other details concerning crystal data and structural refinement are given in Table 1. Structural data can be obtained free of charge from the Cambridge Crystallographic Data Centre via www.ccdc.cam.ac.uk/structures (accessed on 19 April 2024). PLATON (version 110423) was used to obtain some geometrical parameters from the cif files [22].

Table 1. Crystal data and structure refinement.

CCDC number	2260009	2260010
Empirical formula	$C_{90}H_{80}Cl_6Mn_3N_{18}O_{46}$	$C_{90}H_{80}Cl_6Mn_3N_{18}O_{46}$
Moiety formula	$3(C_{30}H_{24}MnN_6O_6)$, $6(ClO_4)$, $4(H_2O)$	$3(C_{30}H_{24}MnN_6O_6)$, $6(ClO_4)$, $4(H_2O)$
Formula weight	2527.24	2527.24
Temperature	100(2) K	100(2) K
Wavelength	0.71073 Å	0.71073 Å
Crystal system	Monoclinic	Monoclinic
Space group	$P2_1/n$	$P2_1/n$
Unit cell dimensions	a = 21.266(2) Å b = 19.1361(16) Å c = 25.447(2) Å $\beta = 90.517(3)^\circ$	a = 21.302(3) Å b = 19.101(3) Å c = 25.487(4) Å $\beta = 90.354(5)^\circ$
Volume	10,355.0(16) Å ³	10,370(2) Å ³
Z	4	4
Density (calculated)	1.621 Mg/m ³	1.619 Mg/m ³
Absorption coefficient	0.620 mm ⁻¹	0.619 mm ⁻¹
F(000)	5164	5132
Crystal size	0.214 × 0.125 × 0.095 mm	0.198 × 0.153 × 0.112 mm
Theta range for data collection	1.915 to 28.407°	1.921 to 28.433°
Index ranges	−28 ≤ h ≤ 28 −25 ≤ k ≤ 25 −33 ≤ l ≤ 33	−28 ≤ h ≤ 28 −25 ≤ k ≤ 25 −33 ≤ l ≤ 33
Reflections collected	591,875	190,729
Independent reflections	25850 [R _{int} = 0.0645, R _σ = 0.0194]	25615 [R _{int} = 0.0759, R _σ = 0.0500]
Reflections observed (>2σ)	22,753	20,710
Data Completeness	0.993	0.980
Absorption correction	Semi-empirical from equivalents	Semi-empirical from equivalents
Max. and min. transmission	0.7144 and 0.6299	0.7457 and 0.6008
Refinement method	Full-matrix least-squares on F ²	Full-matrix least-squares on F ²
Data/restraints/parameters	25,850/0/1483	25,615/0/1468
Goodness-of-fit on F ²	1.069	1.096
Final R indices [I > 2σ(I)]	R ₁ = 0.0531 wR ₂ = 0.1359	R ₁ = 0.1002 wR ₂ = 0.2632
R indices (all data)	R ₁ = 0.0607 wR ₂ = 0.1421	R ₁ = 0.1157 wR ₂ = 0.2710
Largest diff. peak and hole	1.685 and −1.087 e.Å ⁻³	1.681 and −0.722 e.Å ⁻³

2.3. Computational Details

Attempts to carry out computational calculations starting from the experimental crystal structure were carried out at the plane-wave DFT level, using the PBEsol GGA functional [23] in combination with on-the-fly generated norm-conserving pseudopotentials [24], but the structure resulted computationally too demanding for the determination of the band structure. A new simplified file, containing only one $[\text{Mn}(\text{bpyO}_2)_3]^{2+}$ cation and two perchlorate anions, was thus derived from the original .cif file and used for the calculations (lattice parameters: $a = 12.30 \text{ \AA}$, $b = 11.10 \text{ \AA}$, $c = 12.48 \text{ \AA}$, $\alpha = \beta = \gamma = 90^\circ$, cell volume = 1703.89 \AA^3). The relative atomic positions were taken from the original .cif file and left unchanged. The lattice parameters were determined with the aid of preliminary computational optimizations of the simplified cell [25], constraining the angles to 90° and keeping fixed the internal coordinates. The number of resulting explicit electrons was 287. This data file is provided as a .cif file in the Supplementary Materials. The charge was set to zero and the number of unpaired electrons in the unit cell was set to five, according to experimental outcomes. The plane-wave basis cut-off was set at 1380 eV. The Brillouin zone sampling for the self-consistent field calculation was carried out with a $2 \times 2 \times 2$ Monkhorst–Pack grid. The dispersion corrections from Tkatchenko and Scheffler were added [26]. Relativistic effects were accounted through the scalar Koelling–Harmon approximation [27]. The band structure was calculated considering 12 points along the Γ -Z-U-X- Γ path. The software used was CASTEP 20.1 [28–30]. The 3D plots were generated with XCrysDen 1.6 [31,32].

The geometry optimizations of systems formally composed by $[\text{Mn}(\text{bpyO}_2)_3]^{n+}$ cations ($n = 2, 3$) and two perchlorate anions were carried out without symmetry constraints using the TPSS0 hyper-GGA method, with 25% HF exchange [33], in combination with Ahlrichs' def2-TZVP basis set [34], the D4 corrections for London dispersion [35,36], and the C-PCM implicit solvation model (dichloromethane as continuous medium) [37,38]. The "unrestricted" formalism was applied, and the absence of meaningful spin contamination was verified by comparing the computed $\langle S^2 \rangle$ values with the theoretical ones. The IR simulations were carried out using the harmonic approximation [39]. A scaling factor of 0.93 was estimated from the comparison between simulated and observed C-H stretching wavenumbers. The same C-PCM/TPSS0/def2-TZVP method was used to investigate the absorption features of $[\text{Mn}(\text{bpyO}_2)_3](\text{ClO}_4)_2$ employing TDDFT theory [40]. The number of roots considered was 24, with the same multiplicity of the ground state. The output of the TDDFT calculation is provided in .pdf format in the Supplementary Materials. Calculations were carried out using ORCA 5.0.3 [41,42]. The Cartesian coordinates of the DFT-optimized geometry are provided as an .xyz file in the Supplementary Materials. The output files, converted in .molden format, were analysed with Multiwfn, version 3.8, from which the electron-hole distributions were obtained [43,44].

3. Results and Discussion

The complex $[\text{Mn}(\text{bipyO}_2)_3](\text{ClO}_4)_2 \cdot 2\text{H}_2\text{O}$ was prepared by reacting hydrated manganese(II) perchlorate with a slight excess of bipyO₂ in water, according to previously reported methods [1,4]. The carbon and hydrogen elemental analysis data were close to the theoretical values (Anal. calcd for $\text{C}_{30}\text{H}_{28}\text{Cl}_2\text{MnN}_6\text{O}_{16}$: C, 42.17%; H, 3.30%; N, 9.84%. Found: C, 42.00%; H, 3.35%; N, 9.79%). The molar conductivity in acetone at 298 K was $203 \text{ ohm}^{-1}\text{mol}^{-1}\text{cm}^2$, as expected for a 2:1 electrolyte with perchlorate counterions [16]. The value of corrected molar magnetic susceptibility obtained at 298 K was 1.40×10^{-2} c.g.s.u., corresponding to a magnetic moment of 5.8 BM, in line with a high-spin d^5 metal complex of the first transition series with negligible interactions among the paramagnetic centres [45]. Given the strong paramagnetic relaxation [46], scarce information was obtained from the ^1H NMR spectrum in D_2O at 300 K, composed by the superposition of very broad resonances in the aromatic region between 9.0 and 7.0 ppm. No signal attributable to the presence of a diamagnetic free ligand was however detected. The ^1H NMR spectrum was not meaningfully improved by changing the temperature.

The stretching related to the N-O bonds in $[\text{Mn}(\text{bipyO}_2)_3][\text{PtCl}_4]$ was associated in the past with an intense IR band at 1210 cm^{-1} , together with weak shoulders at 1235 and 1225 cm^{-1} . The wavenumbers were lower than those of the free ligand (1262 and 1255 cm^{-1}), an outcome attributed to the weakening of the N-O bonds caused by coordination [2,47]. The IR spectrum of the perchlorate salt here reported (Figure 1) is slightly different compared to previous outcomes, since two bands with comparable intensity are observable in the region generally attributed to the stretching of coordinated N-O bonds, respectively, at 1233 and 1214 cm^{-1} . DFT TPSS0 calculations predicted the N-O stretchings, mixed with C-H bendings, at around 1245 cm^{-1} (scaled value). The number and the relative intensities of the bands in the experimental spectrum thus almost appear in part related to the choice of the counteranion and to solid-state effects. On considering other selected portions of the spectrum, the perchlorate anions are associated with an intense band centred at 1092 cm^{-1} . The $\nu_{\text{O-H}}$ stretching region is composed of two bands and a shoulder, respectively, at 3594 , 3504 and 3430 cm^{-1} because of the presence of lattice water molecules. The related HOH bending vibrations correspond to a convolution of bands centred at 1626 cm^{-1} [47].

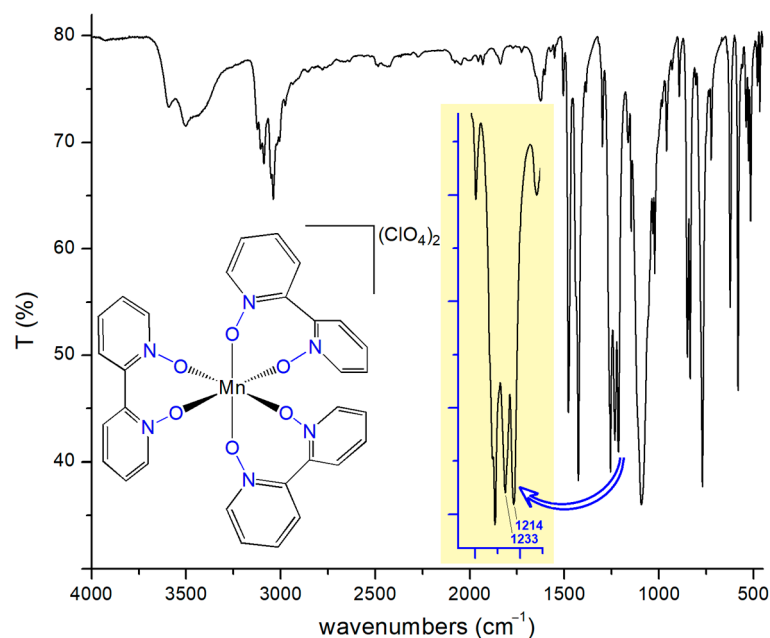


Figure 1. IR spectrum (KBr) of the hydrated perchlorate salt of $[\text{Mn}(\text{bipyO}_2)_3]^{2+}$ with N-O stretching highlighted.

Slow evaporation of water solutions allowed the isolation of single crystals suitable for X-ray diffraction. The compound crystallizes in the monoclinic system, $P2_1/n$ space group ($Z = 4$), and the asymmetric unit contains three cationic complexes, six perchlorate anions and an undetermined number of water molecules (see the Section 2.2). The resulting cationic complexes in the crystal structure were manganese(II) ions coordinated by three chelating 2,2'-bipyridine 1,1'-dioxide ligands. The ORTEP drawing of one of the cations is shown in Figure 2. Figure 3 shows the asymmetric unit content. The environment of the manganese(II) ions is best defined as octahedral with scarce variations among the three cations in the asymmetric unit, as confirmed by the output of the Shape program reported in Table 2 [48]. Consequently, as observable in Figure 3, the three complexes are almost super-imposable. Salient bond lengths and angles are collected in Table 3.

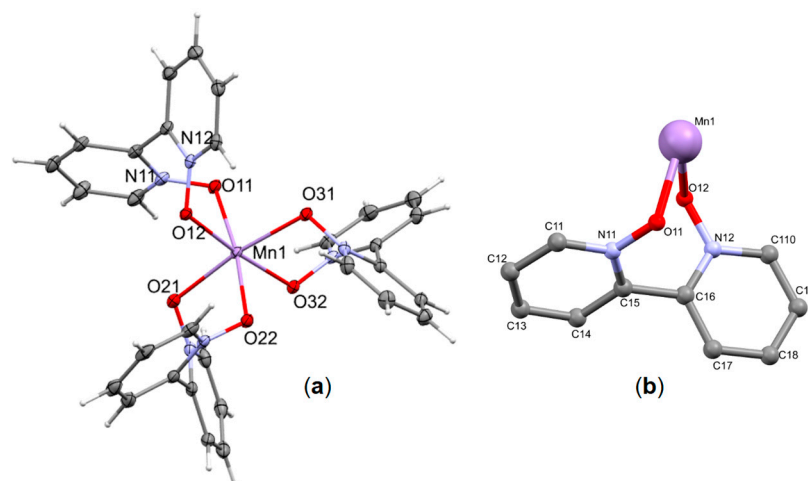


Figure 2. (a) X-ray structure of one of the $[\text{Mn}(\text{bipyO}_2)]^{2+}$ cations. Color map: Mn, violet; O, red; N, blue; C, grey; H, white. (b) Coordinative fashion of the ligand. Hydrogen atoms are omitted for clarity. All other ligands were labeled following the same scheme.

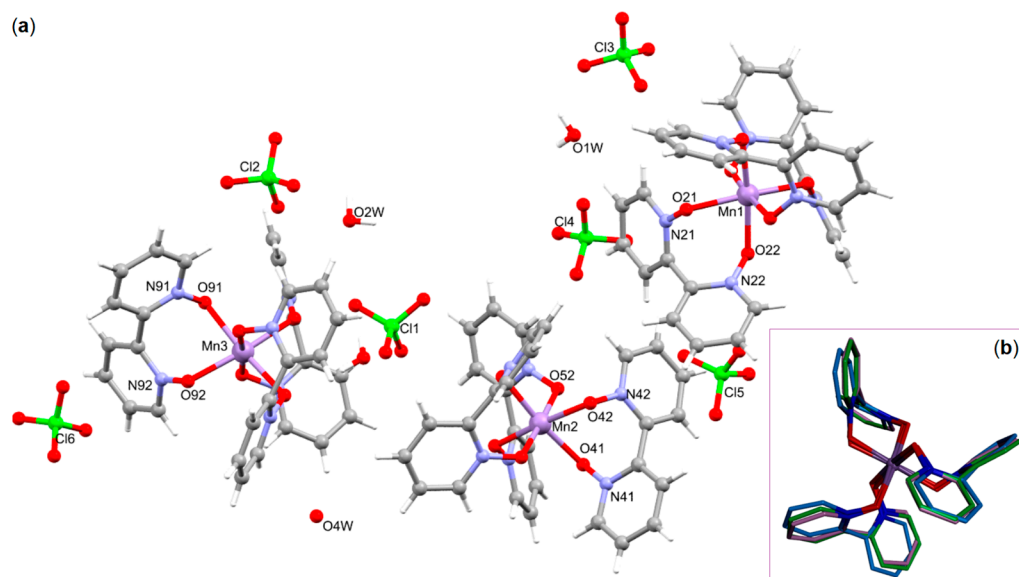


Figure 3. (a) Asymmetric unit of the crystal structure. Color map: Mn, violet; Cl, green; O, red; N, blue; C, grey; H, white. For the sake of clarity, only selected atoms were labeled to show the labelling scheme. (b) Superimposition of the three cationic molecules found in the asymmetric unit. Hydrogen atoms are omitted for clarity and the three complexes are distinguished using different colors for the carbon atoms (blue, green and violet).

Table 2. Output of the SHAPE version 2.1 [49] Continuous Shape Measures calculations.

Metal Centre in $[\text{Mn}(\text{bpyO}_2)_3]^{2+}$	HP-6 ¹	PPY-6 ²	OC-6 ³	TPR-6 ⁴	JPPY-6 ⁵
Mn(1)	31.434	26.431	0.448	13.827	29.948
Mn(2)	28.939	26.779	0.480	13.878	30.329
Mn(3)	28.559	25.277	0.549	13.234	28.607

¹ HP-6, D_{6h} Hexagon. ² PPY-6, C_{5v} Pentagonal pyramid. ³ C-6, O_h Octahedron. ⁴ TPR-6, D_{3h} Trigonal prism. ⁵ JPPY-6, C_{5v} Johnson pentagonal pyramid J2.

Table 3. Selected bond lengths (Å) and angles (°) for the cationic complexes in CCDC 2260009.

Mn(1)-O(11)	2.1594(18)	Mn(2)-O(41)	2.1704(19)	Mn(3)-O(71)	2.160(2)
Mn(1)-O(12)	2.1409(17)	Mn(2)-O(42)	2.1475(18)	Mn(3)-O(72)	2.1080(19)
Mn(1)-O(21)	2.1585(19)	Mn(2)-O(51)	2.1393(18)	Mn(3)-O(81)	2.1329(18)
Mn(1)-O(22)	2.1585(18)	Mn(2)-O(52)	2.1446(17)	Mn(3)-O(82)	2.1387(17)
Mn(1)-O(31)	2.1553(18)	Mn(2)-O(61)	2.1658(19)	Mn(3)-O(91)	2.175(2)
Mn(1)-O(32)	2.1359(17)	Mn(2)-O(62)	2.1230(18)	Mn(3)-O(92)	2.143(2)
O(11)-N(11)	1.336(3)	O(41)-N(41)	1.323(3)	O(71)-N(71)	1.339(3)
O(12)-N(12)	1.326(3)	O(42)-N(42)	1.337(3)	O(72)-N(72)	1.313(3)
O(21)-N(21)	1.329(3)	O(51)-N(51)	1.332(3)	O(81)-N(81)	1.331(2)
O(22)-N(22)	1.328(3)	O(52)-N(52)	1.324(3)	O(82)-N(82)	1.333(3)
O(31)-N(31)	1.335(3)	O(61)-N(61)	1.333(3)	O(91)-N(91)	1.327(3)
O(32)-N(32)	1.331(3)	O(62)-N(62)	1.333(3)	O(92)-N(92)	1.324(3)
O(12)-Mn(1)-O(11)	84.31(7)	O(42)-Mn(2)-O(41)	84.80(7)	O(71)-Mn(3)-O(91)	173.66(8)
O(12)-Mn(1)-O(21)	94.61(7)	O(42)-Mn(2)-O(61)	91.29(7)	O(72)-Mn(3)-O(71)	85.15(7)
O(12)-Mn(1)-O(22)	91.66(7)	O(51)-Mn(2)-O(41)	90.07(7)	O(72)-Mn(3)-O(81)	99.51(7)
O(12)-Mn(1)-O(31)	91.19(7)	O(51)-Mn(2)-O(42)	174.46(7)	O(72)-Mn(3)-O(82)	175.03(8)
O(21)-Mn(1)-O(11)	90.63(7)	O(51)-Mn(2)-O(52)	84.03(7)	O(72)-Mn(3)-O(91)	90.36(7)
O(21)-Mn(1)-O(22)	82.97(7)	O(51)-Mn(2)-O(61)	93.62(7)	O(72)-Mn(3)-O(92)	84.03(8)
O(22)-Mn(1)-O(11)	172.15(7)	O(52)-Mn(2)-O(41)	80.96(7)	O(81)-Mn(3)-O(71)	86.75(7)
O(31)-Mn(1)-O(11)	95.44(7)	O(52)-Mn(2)-O(42)	93.08(7)	O(81)-Mn(3)-O(82)	85.38(7)
O(31)-Mn(1)-O(21)	171.99(7)	O(52)-Mn(2)-O(61)	93.84(7)	O(81)-Mn(3)-O(91)	89.59(7)
O(31)-Mn(1)-O(22)	91.36(7)	O(61)-Mn(2)-O(41)	173.29(7)	O(81)-Mn(3)-O(92)	173.23(8)
O(32)-Mn(1)-O(11)	96.00(7)	O(62)-Mn(2)-O(41)	100.48(7)	O(82)-Mn(3)-O(71)	96.05(7)
O(32)-Mn(1)-O(12)	174.59(7)	O(62)-Mn(2)-O(42)	88.26(7)	O(82)-Mn(3)-O(91)	88.80(7)
O(32)-Mn(1)-O(21)	90.80(7)	O(62)-Mn(2)-O(51)	94.75(7)	O(82)-Mn(3)-O(92)	91.01(7)
O(32)-Mn(1)-O(22)	88.66(7)	O(62)-Mn(2)-O(52)	178.13(7)	O(92)-Mn(3)-O(71)	99.35(8)
O(32)-Mn(1)-O(31)	83.40(7)	O(62)-Mn(2)-O(61)	84.81(7)	O(92)-Mn(3)-O(91)	84.60(8)
N(11)-O(11)-Mn(1)	114.40(14)	N(41)-O(41)-Mn(2)	115.98(14)	N(71)-O(71)-Mn(3)	114.30(15)
N(12)-O(12)-Mn(1)	118.29(14)	N(42)-O(42)-Mn(2)	110.68(13)	N(72)-O(72)-Mn(3)	117.94(16)
N(21)-O(21)-Mn(1)	112.93(14)	N(51)-O(51)-Mn(2)	113.79(14)	N(81)-O(81)-Mn(3)	113.71(14)
N(22)-O(22)-Mn(1)	117.12(14)	N(52)-O(52)-Mn(2)	116.13(14)	N(82)-O(82)-Mn(3)	113.63(13)
N(31)-O(31)-Mn(1)	113.21(14)	N(61)-O(61)-Mn(2)	113.21(14)	N(91)-O(91)-Mn(3)	112.43(14)
N(32)-O(32)-Mn(1)	120.55(14)	N(62)-O(62)-Mn(2)	118.81(14)	N(92)-O(92)-Mn(3)	113.25(15)

Structurally characterized transition metal homoleptic complexes with the bipyO₂ ligand are scarce. Among the few examples found in the literature, it is worth mentioning the Cu(II) complex [Cu(bipyO₂)₃]²⁺, obtained in hydrated form either as perchlorate [50] or as tetrafluoroborate salt [51]. Another example concerning the first transition metals series is the iron(III) complex [Fe(bipyO₂)₃]³⁺, also in this case isolated as perchlorate salt [52]. Some eight-coordinated trivalent lanthanoid (Ln) complexes were also published. In particular, [La(bipyO₂)₄](ClO₄)₃ represents a rare example of cubic coordination involving a Ln³⁺ ion [53]. Related complexes containing smaller lanthanide ions showed distorted dodecahedral and square anti-prismatic structures [54,55]. Structurally characterized bipyO₂ derivatives include heteroleptic species. Selected examples show the ligand coordinated to a lanthanide ion, to a main group metal such as bismuth, or to a Group 12 element [56–58]. In all the cited compounds, bipyO₂ behaves as a chelating ligand. As recently summarized [58], other possible coordination modes, such as bridging or transoid, are possible, even if structurally characterized compounds are scarce. An example is the coordination polymer [Cu₂(O₂CC₆H₅)₄(bipyO₂)_n] [59], where bipyO₂ bridges di-nuclear copper(II) {Cu₂(O₂CC₆H₅)₄} fragments.

In the compound here investigated, the dihedral angles between the pyridine rings are in the 61.8(2)°–71.7(2)° range. The average value is 65.3(2)°, similar to that found in the free ligand, 67.5°, which also adopts a skew conformation [60], or in its hydrate, 70.1° [61]. The dihedral angle is, however, also comparable if the ligand behaves as bridge, as observed in the previously mentioned copper(II) coordination polymer (67.12°) [59]. The O---O distance appears, thus, a better indicator of the changes associated with the

coordination, being 3.046(2) Å in the free ligand and 3.104 Å in the corresponding hydrate form. The average value found in the manganese(II) complex here described is shorter, 2.885(3) Å while, in the copper(II) transoid complex, it is longer than 4 Å. As expected, the seven-membered chelate ring is significantly puckered (see Figure 2). The Mn-O distances, between 2.108(2) and 2.175(2) Å, average 2.147(2) Å, are similar to those found in $[\text{Mn}\{\text{NC-C}(\text{CN})_2\}_2(\text{bipyO}_2)_2]$, 2.1290(13) and 2.1780(13) Å [62], while the chelate angles are between 82.97(7) and 85.38(7)°, average 84.38(8)°, slightly bigger than the 82.30(4)° found in previously mentioned heteroleptic tricyanomethanido complex. The M-O bond lengths are shorter than those found in the manganese(II) polymeric compound obtained by reacting hydrated manganese(II) acetate with 2,2'-bipyridine-3,3'-dicarboxylic acid 1,1'-dioxide, 2.194(2) and 2.208(2) Å, where the ligand both chelates and bridges the metal centres due to the presence of the additional carboxylic groups [63]. To the best of our knowledge, these two compounds complete the list of crystallographic studied chelating bipyO₂ manganese(II) complexes [64].

Initial computational investigations on the electronic structure of the compound were carried out on the simplified .cif file, where only one $[\text{Mn}(\text{bipyO}_2)_3]^{2+}$ cation and two perchlorate anions were maintained (see the Supporting Materials for further information). The number of unpaired electrons was set to five based on the previously described magnetic measurements. Both the *alpha* and *beta* band structures were obtained, but the first one is more interesting, since *alpha* spin was attributed to the unpaired electrons. The *alpha* band structure close to the valence (VB) and conduction (CB) bands is reported in Figure 4, together with the density of states (DOS), separated by the orbital type. Partial DOS related to the d-type orbitals of the manganese center is associated either with the bands immediately below the VB or with a group of bands comprised between −1.4 and −1.7 eV. The d-type DOS is much reduced for the occupied bands at lower energy, and it is scarce for the CB and the empty bands above. The plots of the bands improved the description of the electronic structure. VB, VB-1 and VB-2 are localized on the oxygen atoms of the perchlorate anions. The bands VB-3 and VB-4 maintain the same character, with minimal contribution of Mn-centred d-type functions. VB-5 and VB-6 have mixed characters, localized on the perchlorate oxygen atoms, on the manganese(II) d-type orbitals, and on the p-orbitals of the coordinating oxygen atoms. The contribution of the metal center becomes dominant in the bands between VB-7 (relative energy around −0.45 eV) and VB-10 (relative energy around −1.66 eV), with the participation of the coordinating bipyO₂ ligands, the donor atoms in particular. This last outcome suggests a non-negligible nephelauxetic effect in the $[\text{Mn}(\text{bipyO}_2)_3]^{2+}$ cation. The manganese center is scarcely involved in the occupied bands, having energy below −2 eV, mainly centred on the bipyO₂ ligands. The CB and the empty bands immediately above are dominated by π -delocalized orbitals on bipyO₂, with the superposition of p-type orbitals of the aromatic rings and the oxygen atoms. Selected bands are shown in Figure 5.

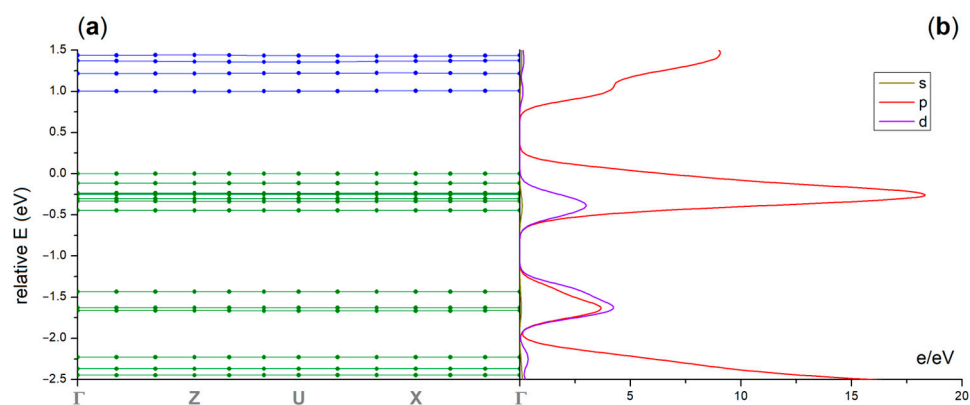


Figure 4. (a) Occupied (green) and empty (blue) bands close to the VB and CB. The energy of the VB is set at 0.0 eV. (b) Plot of the orbital contributions (s, p, d) to the DOS.

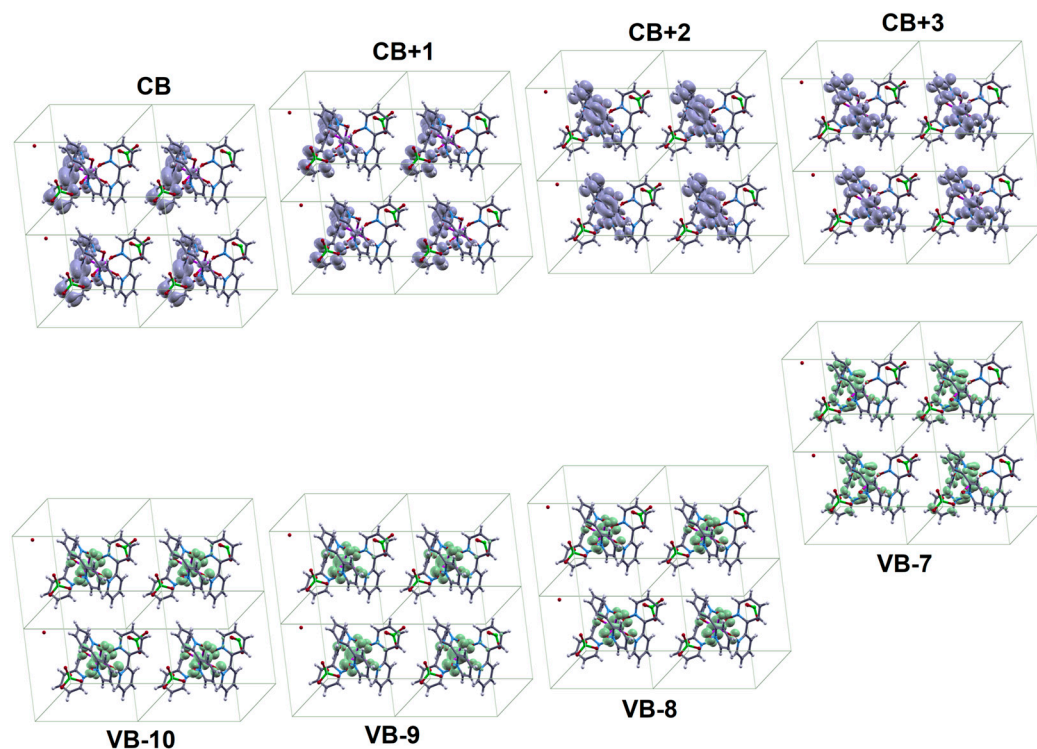


Figure 5. Density plots of selected occupied and empty bands (surface iso-value = 0.01 a.u.). Color map: Mn, violet; Cl, green; O, red; N, blue; C, grey; H, white. The surfaces are plotted in green and blue tones for the occupied and empty bands, respectively.

The results of the plane-wave DFT calculations suggest that the transitions responsible for the absorption of the complex in the visible range could be ascribed to spin-allowed transitions from metal-centred occupied orbitals to bipyO₂-centred unoccupied orbitals, in agreement with previous hypotheses [4,6]. The MLCT nature of the absorption was further corroborated by non-periodic C-PCM/TPSS0/def2-TZVP calculations on [Mn(bipyO₂)₃](ClO₄)₂. Sextet multiplicity was considered, given the high-spin d⁵ electronic configuration of the metal centre derived from the magnetic measurements. The optimized geometry is shown in Figure 6 together with the spin density plot. The root-mean-square-deviation (RMSD) of the optimized [Mn(bipyO₂)₃]²⁺ cation compared to the starting experimental structure is quite low, at 0.521 Å. The Mn–O bond lengths are in the 2.118–2.158 Å range. The O–Mn–O angles are between 167.5 and 177.3° (*trans*) and between 81.9 and 98.9° (*cis*). Selected average computed bond lengths and angles are collected in the caption of Figure 6. The spin density plot confirms that the unpaired electrons are essentially localized on the metal center, even if limited spin density can be observed also on the coordinated ligands. Starting from the optimized stationary point, TDDFT calculations predicted the wavelengths of the two spin-allowed transitions at 438 and 430 nm, i.e., in the interval experimentally observed [4,6], with oscillator strengths, respectively, equal to 0.090 and 0.067. The molecular orbitals mostly involved in the transitions are the occupied α -HOMO and α -HOMO-1 and the unoccupied α -LUMO, α -LUMO+1 and α -LUMO+2. α -HOMO and α -HOMO-1 show an important contribution of d-type orbitals on the manganese center, which give σ -antibonding interactions with the coordinated ligands. The percentage of metal contribution is 38% in α -HOMO and 29% in α -HOMO-1, while the contributions of the six coordinating oxygen atoms are 33% and 27%, respectively, for α -HOMO and α -HOMO-1. On the contrary, the participation of the metal ion in the empty orbitals is limited and is between 0% and 3%. α -LUMO, α -LUMO+1 and α -LUMO+2 are essentially π^* orbitals of the bipyO₂ ligands, as already stated from the plane-wave DFT calculations (Figure 6). The MLCT nature of the transitions can be better represented using the hole-electron distributions associated with the two transitions, as observable in Figure 7.

It is worth noting that the orbitals of the coordinating oxygen atoms participate in both the hole and the electron surfaces.

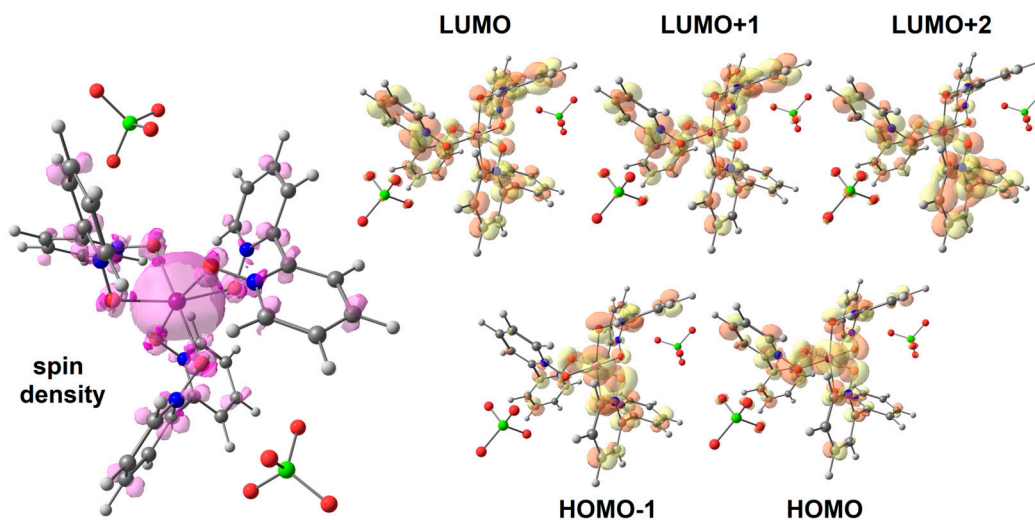


Figure 6. DFT-optimized geometry of $[\text{Mn}(\text{bipyO}_2)_3](\text{ClO}_4)_2$ (sextet state) with spin density surface (violet tones, iso-value = 0.002 a.u.) and molecular orbitals plots from HOMO-1 to LUMO+2 (yellow and orange tones, iso-value = 0.03 a.u.). Color map: Mn, violet; Cl, green; O, red; N, blue; C, grey; H, white. Selected average computed bond lengths (\AA): Mn-O 2.140; O-N 1.306. Selected average computed bond angles ($^\circ$): O-Mn-O 171.4 (*trans*); O-Mn-O 90.2 (*cis*).

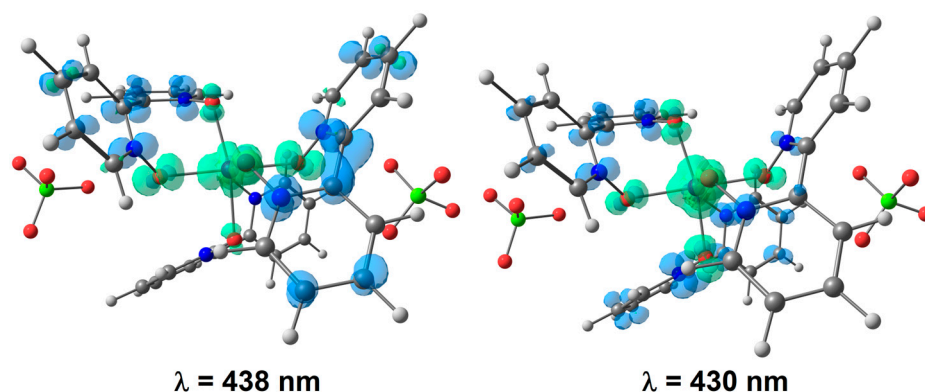


Figure 7. Hole (green tones) and electron (blue tones) distributions for the transitions predicted at 438 and 430 nm (surfaces' iso-value = 0.003 a.u.). Color map: Mn, violet; Cl, green; O, red; N, blue; C, grey; H, white.

The vibrational decay from the MLCT excited state appears to be a fast process since no luminescence was observed in solution or in the solid state. Non-radiative routes must also be competitive to the intersystem, crossing towards excited states with different multiplicity, since no metal-centred transition was observed. For completeness, the quartet excited state of $[\text{Mn}(\text{bipyO}_2)_3](\text{ClO}_4)_2$ was calculated starting from the sextet ground state geometry and was energetically higher by about 1.73 eV, corresponding to a transition around 720 nm. The computed value is in line with d-d transitions of manganese(II) in an octahedral field [65,66] and the spin density remains localized at the metal center.

Another decay route is the photodecomposition of the complex, as already stated [7]. Irradiation of dichloromethane solutions of the complex with a LED source centred at 405 nm caused the progressive disappearance of the MLCT band between 400 and 500 nm and the increase in the bands below 400 nm, as observable in Figure 8. The same behaviour was observed using acetonitrile as solvent. The decomposition can be rationalized based on the molecular orbitals depicted in Figure 6. Upon excitation, the N-O bonds are weakened

by the depopulation of σ -antibonding Mn-O orbitals and the consequent population of π -antibonding bipyO₂ orbitals [8].

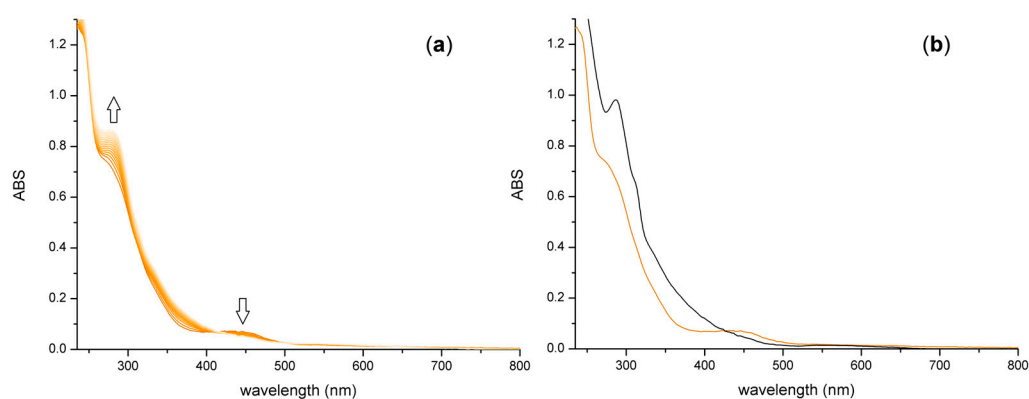


Figure 8. (a) Changes of the absorption spectrum of [Mn(bipyO₂)₃](ClO₄)₂ during 5 min of irradiation at 405 nm. (b) Comparison between the initial spectrum of the complex (orange line) and after 25 min of irradiation (black line). CH₂Cl₂, 298 K.

An intriguing feature of the complex, connected with the MLCT absorption, is its redox behaviour, the quasi-reversible oxidation processes in particular. The electrochemical measurements carried out in this work confirmed the previous results [6]. Figure 9 shows the superposition of the cyclic voltammograms of [Mn(bipyO₂)₃](ClO₄)₂ and bipyO₂ under the same experimental conditions. Two oxidation processes at $E_{1/2} = 0.48$ V and 1.21 V vs. Fc⁺/Fc are clearly observable for the complex, absent in the cyclic voltammogram of the free ligand. Previous investigations of [Mn(bipyO₂)₃]²⁺ and the related [Mn(terpyO₃)₂]²⁺ cation (terpyO₃ = 2,2',2''-terpyridine 1,1',1''-trioxide) strongly support that the two processes in the anodic region are attributable to the Mn(II)/Mn(III) and Mn(III)/Mn(IV) redox couples [6]. On the other hand, the peak centred at -1.95 V vs. Fc⁺/Fc, with the associated reverse process at -1.17 V vs. Fc⁺/Fc, corresponds to a reduction centred on the coordinated ligands, as deducible from the comparison with the cyclic voltammogram of free bipyO₂. Focusing the attention on the first oxidation, the good reversibility of the process can almost in part be ascribed to small structural changes in the complex after the removal of one electron. The DFT-optimized structure of [Mn(bipyO₂)₃]³⁺ (quintet state) is almost superimposable with that computed for the parent cation, the RMSD equal to 0.267 Å (see also Figure 9), despite the prolate first coordination sphere due to the Jahn–Teller distortion. The spin density remains mostly localized on the metal center. The Mn–O bond lengths are in the 1.905–2.139 Å range. The average value is 1.998 Å, 0.142 Å shorter than that computed for [Mn(bipyO₂)₃]²⁺. The average O–Mn–O angles are 176.4° (trans) and 90.0° (cis). The change in oxidation state does not meaningfully affect the N–O bonds, since the average value in [Mn(bipyO₂)₃]³⁺ is 1.324 Å, only 0.018 Å longer than that computed for [Mn(bipyO₂)₃]²⁺. On the other hand, the removal of one electron alters the composition of the frontier orbitals with respect to the parent cation. Both α -HOMO and α -LUMO present a meaningful participation of metal-centred orbitals, equal to 21% in α -HOMO and 32% in α -LUMO.

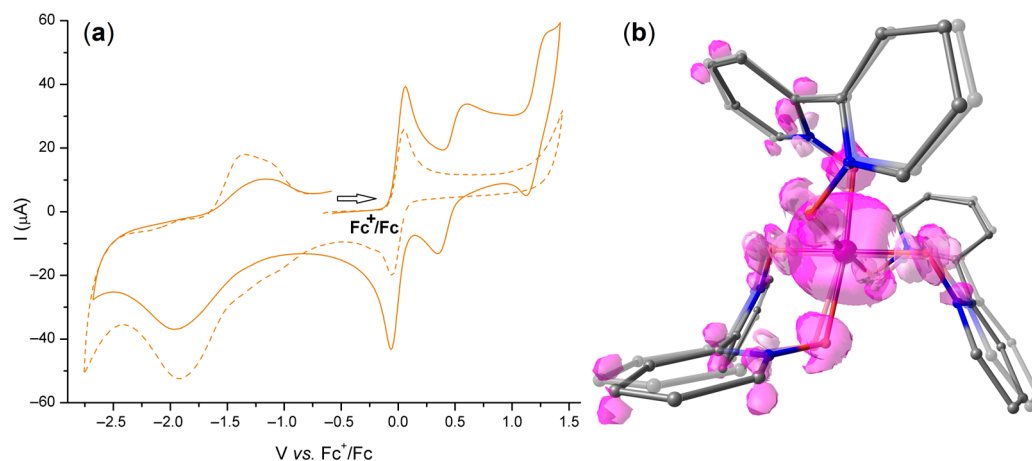


Figure 9. (a) Cyclic voltammograms of $[\text{Mn}(\text{bipyO}_2)_3](\text{ClO}_4)_2$ (solid line) and bipyO_2 (dashed line). $\text{CH}_3\text{CN}/\text{LiClO}_4$, r.t., Fc as internal standard, scan rate 1 V s^{-1} . (b) DFT-optimized geometry of $[\text{Mn}(\text{bipyO}_2)_3]^{3+}$ (quintet state) with spin density surface (violet tones, iso-value = 0.002 a.u.), superimposed to the DFT-optimized geometry of the parent cation $[\text{Mn}(\text{bipyO}_2)_3]^{2+}$ (transparent). Color map: Mn, violet; Cl, green; O, red; N, blue; C, grey; H, white.

4. Conclusions

The results provided in this work increased our knowledge of the cationic complex $[\text{Mn}(\text{bipyO}_2)_3]^{2+}$ through the single-crystal X-ray structure determination of its perchlorate salt. Moreover, DFT and TDDFT calculations helped to shed light on the electronic structure and, thus, on the peculiar optical and electrochemical behaviour. The ease of synthesis and the solubility in different solvents make $[\text{Mn}(\text{bipyO}_2)_3]^{2+}$ of potential interest as selective reducing agent, and the possibility of light-driven reactions will be explored in further studies.

Supplementary Materials: The following supporting information can be downloaded at: <https://www.mdpi.com/article/10.3390/cryst14050422/s1>, MnBipyO2_ClO4.cif: single-crystal structure .cif files; checkcif.pdf: single-crystal structure checkcif files; Mn_simplified.cif: simplified structure for plane-wave calculations; TDDFT.pdf: output of the TDDFT calculation; DFT-coordinates.xyz: Cartesian coordinates of the DFT-optimized structures.

Author Contributions: Conceptualization, M.B.; methodology, J.C. and M.B.; validation, J.C., M.B. and V.F.; formal analysis, J.C., V.F. and M.B.; investigation, J.C., M.B. and V.F.; resources, J.C., M.B. and V.F.; data curation, J.C., M.B. and V.F.; writing—original draft preparation, M.B. and J.C.; writing—review and editing, J.C., M.B. and V.F.; visualization, M.B. and J.C.; supervision, M.B.; project administration, M.B.; funding acquisition, M.B. All authors have read and agreed to the published version of the manuscript.

Funding: This study was funded by Università Ca' Foscari Venezia, Bando Spin 2018, D. R. 1065/2018 prot. 67416. This work is part of the “Network 4 Energy Sustainable Transition-NEST” project (MIUR project code PE000021, Concession Degree No. 1561 of 11 October 2022), in the framework of the NextGenerationEu PNRR plan (CUP C93C22005230007).

Data Availability Statement: Data are contained within the article and Supplementary Materials.

Acknowledgments: CACTI (University of Vigo) and CINECA (Bologna) are respectively acknowledged for X-ray data collection and the availability of high-performance computing resources (class C projects COLUMN21, COLUMN22 and INLIGHT). We sincerely thank Fabio Marchetti (Università di Pisa) for the availability of the academic version of CASTEP.

Conflicts of Interest: The authors declare no conflicts of interest. The funders had no role in the design of the study; in the collection, analyses, or interpretation of data; in the writing of the manuscript; or in the decision to publish the results.

References

1. Simpson, P.G.; Vinciguerra, A.; Quagliano, J.V. The Donor Properties of 2,2'-Bipyridine N,N'-Dioxide. *Inorg. Chem.* **1963**, *2*, 282–286. [[CrossRef](#)]
2. Vinciguerra, A.; Simpson, P.G.; Kakiuti, Y.; Quagliano, J.V. Infrared Studies of 2,2'-Bipyridine N,N'-Dioxide and its Metal Complexes in the 3–38 μ Region. *Inorg. Chem.* **1963**, *2*, 286–289. [[CrossRef](#)]
3. Nyholm, R.S.; Turco, A. Tervalent Manganese Complexes of 2,2'-Bipyridyl 1,1-Dioxide. *J. Chem. Soc.* **1962**, 1121–1122. [[CrossRef](#)]
4. Madan, S.K.; Bull, W.E. Metallic complexes of 2,2'-bipyridine-1,1'-dioxide. *J. Inorg. Nucl. Chem.* **1964**, *26*, 2211–2217. [[CrossRef](#)]
5. Ahuja, I.S.; Singh, R.; Yadava, C.L. Structural information on manganese(II) chloride, thiocyanate, acetate and sulphate complexes with 2,2'-bipyridyl, 4,4'-bipyridyl and their dioxides from their magnetic moments, electronic and infrared spectra. *J. Mol. Struct.* **1981**, *74*, 143–151. [[CrossRef](#)]
6. Morrison, M.M.; Sawyer, S.T. 2,2'-Bipyridine 1,1'-Dioxide and 2,2',2''-Terpyridine 1,1',1''-Trioxide Complexes of Manganese(II), -(III), and -(IV). *Inorg. Chem.* **1978**, *17*, 338–339. [[CrossRef](#)]
7. Garvery, R.G.; Nelson, J.H.; Ragsdale, R.O. The coordination chemistry of aromatic amine N-oxides. *Coord. Chem. Rev.* **1968**, *3*, 375–407. [[CrossRef](#)]
8. Nathan, L.C.; Cullen, J.; Ragsdale, R.O. Decomposition studies of amine N-oxide manganese(II) complexes. *Inorg. Nucl. Chem. Lett.* **1976**, *12*, 137–140. [[CrossRef](#)]
9. Wu, Y.; Zhang, X.; Xu, L.-J.; Yang, M.; Chen, Z.-N. Luminescent Vapochromism Due to a Change of the Ligand Field in a One-Dimensional Manganese(II) Coordination Polymer. *Inorg. Chem.* **2018**, *57*, 9175–9181. [[CrossRef](#)]
10. Berezin, A.-S.; Samsonenko, D.G.; Brel, V.K.; Artem'ev, A.V. "Two-in-one" organic–inorganic hybrid Mn^{II} complexes exhibiting dual-emissive phosphorescence. *Dalton Trans.* **2018**, *47*, 7306–7315. [[CrossRef](#)]
11. Bortoluzzi, M.; Castro, J.; Trave, E.; Dallan, D.; Favaretto, S. Orange-emitting manganese(II) complexes with chelating phosphine oxides. *Inorg. Chem. Commun.* **2018**, *90*, 105–107. [[CrossRef](#)]
12. Koshino, N.; Kuchiyama, Y.; Ozaki, H.; Funahashi, S.; Takagi, H.D. An Interpretation of Gated Behavior: Kinetic Studies of the Oxidation and Reduction Reactions of Bis(2,9-dimethyl-1,10-phenanthroline)copper(I/II) in Acetonitrile. *Inorg. Chem.* **1999**, *38*, 3352–3360. [[CrossRef](#)]
13. Willams, D.B.G.; Lawton, M. Drying of Organic Solvents: Quantitative Evaluation of the Efficiency of Several Desiccants. *J. Org. Chem.* **2010**, *75*, 8351–8354. [[CrossRef](#)]
14. Peng, X.; Huang, P.; Jiang, L.; Zhu, J.; Liu, L. Palladium-catalyzed highly regioselective oxidative homocoupling of 1,2,3-triazole N-oxides. *Tetrahedron Lett.* **2016**, *57*, 5223–5226. [[CrossRef](#)]
15. Bain, G.A.; Berry, J.F. Diamagnetic corrections and Pascal's constants. *J. Chem. Educ.* **2008**, *85*, 532–536. [[CrossRef](#)]
16. Geary, W.J. The use of conductivity measurements in organic solvents for the characterization of coordination compounds. *Coord. Chem. Rev.* **1971**, *7*, 81–122. [[CrossRef](#)]
17. Elgrishi, N.; Rountree, K.J.; McCarthy, B.D.; Rountree, E.S.; Eisenhart, T.T.; Dempsey, J.L. A Practical Beginner's Guide to Cyclic Voltammetry. *J. Chem. Ed.* **2018**, *95*, 197–206. [[CrossRef](#)]
18. Bruker AXS Inc. APEX4, SMART, SAINT; Bruker AXS Inc.: Madison, WI, USA, 2022.
19. McArdle, P. Oscail, a program package for small-molecule single-crystal crystallography with crystal morphology prediction and molecular modelling. *J. Appl. Crystallogr.* **2017**, *50*, 320–326. [[CrossRef](#)]
20. Sheldrick, G.M. SHELXT—Integrated space-group and crystal-structure determination. *Acta Crystallogr.* **2015**, *A71*, 3–8. [[CrossRef](#)]
21. Sheldrick, G.M. Crystal structure refinement with SHELXL. *Acta Crystallogr.* **2015**, *C71*, 3–8. [[CrossRef](#)]
22. Spek, A.L. checkCIF validation ALERTS: What they mean and how to respond. *Acta Crystallogr.* **2020**, *E76*, 1–11. [[CrossRef](#)] [[PubMed](#)]
23. Perdew, J.P.; Ruzsinszky, A.; Csonka, G.I.; Vydrov, O.A.; Scuseria, G.E.; Constantin, L.A.; Zhou, X.; Burke, K. Restoring the Density-Gradient Expansion for Exchange in Solids and Surfaces. *Phys. Rev. Lett.* **2008**, *100*, 136406. [[CrossRef](#)] [[PubMed](#)]
24. Lin, J.S.; Qteish, A.; Payne, M.C.; Heine, V. Optimized and transferable nonlocal separable ab initio pseudopotentials. *Phys. Rev. B* **1993**, *47*, 4174–4180. [[CrossRef](#)] [[PubMed](#)]
25. Pfrommer, B.G.; Côté, M.; Louie, S.G.; Cohen, M.L. Relaxation of Crystals with the Quasi-Newton Method. *J. Comput. Phys.* **1997**, *131*, 233–240. [[CrossRef](#)]
26. Tkatchenko, A.; Scheffler, M. Accurate Molecular Van Der Waals Interactions from Ground-State Electron Density and Free-Atom Reference Data. *Phys. Rev. Lett.* **2009**, *102*, 073005. [[CrossRef](#)] [[PubMed](#)]
27. Koelling, D.D.; Harmon, B.N. A technique for relativistic spin-polarised calculations. *J. Phys. C Solid State Phys.* **1977**, *10*, 3107–3114. [[CrossRef](#)]
28. Clark, S.J.; Segall, M.D.; Pickard, C.J.; Hasnip, P.J.; Probert, M.I.J.; Refson, K.; Payne, M.C. First principles methods using CASTEP. *Z. Kristallogr.* **2005**, *220*, 567–570. [[CrossRef](#)]
29. Rutter, M.J. C2x: A tool for visualisation and input preparation for Castep and other electronic structure codes. *Comput. Phys. Commun.* **2018**, *225*, 174–179. [[CrossRef](#)]
30. Hinuma, Y.; Pizzi, G.; Kumagai, Y.; Oba, F.; Tanaka, I. Band structure diagram paths based on crystallography. *Comput. Mater. Sci.* **2017**, *128*, 140–184. [[CrossRef](#)]
31. Kokalj, A. Computer graphics and graphical user interfaces as tools in simulations of matter at the atomic scale. *Comput. Mater. Sci.* **2003**, *28*, 155–168. [[CrossRef](#)]

32. Kokalj, A. XCrySDen—A new program for displaying crystalline structures and electron densities. *J. Mol. Graph. Model.* **1999**, *17*, 176–179. [[CrossRef](#)] [[PubMed](#)]
33. Staroverov, V.N.; Scuseria, E.; Tao, J.; Perdew, J.P. Comparative assessment of a new nonempirical density functional: Molecules and hydrogen-bonded complexes. *J. Chem. Phys.* **2003**, *119*, 12129–12137. [[CrossRef](#)]
34. Weigend, F.; Ahlrichs, R. Balanced basis sets of split valence, triple zeta valence and quadruple zeta valence quality for H to Rn: Design and assessment of accuracy. *Phys. Chem. Chem. Phys.* **2005**, *7*, 3297–3305. [[CrossRef](#)] [[PubMed](#)]
35. Caldeweyher, E.; Bannwarth, C.; Grimme, S. Extension of the D3 dispersion coefficient model. *J. Chem. Phys.* **2017**, *147*, 034112. [[CrossRef](#)] [[PubMed](#)]
36. Caldeweyher, E.; Ehlert, S.; Hansen, A.; Neugebauer, H.; Spicher, S.; Bannwarth, C.; Grimme, S. A generally applicable atomic charge dependent London dispersion correction. *J. Chem. Phys.* **2019**, *150*, 154122. [[CrossRef](#)] [[PubMed](#)]
37. Cossi, M.; Rega, N.; Scalmani, G.; Barone, V. Energies, structures, and electronic properties of molecules in solution with the C-PCM solvation model. *J. Comput. Chem.* **2003**, *24*, 669–681. [[CrossRef](#)] [[PubMed](#)]
38. Barone, V.; Cossi, M. Quantum calculation of molecular energies and energy gradients in solution by a conductor solvent model. *J. Phys. Chem. A* **1998**, *102*, 1995–2001. [[CrossRef](#)]
39. Cramer, C.J. *Essentials of Computational Chemistry*, 2nd ed.; Wiley: Chichester, UK, 2004.
40. Ullrich, C.A. *Time-Dependent Density Functional Theory*; Oxford University Press: Oxford, UK, 2012.
41. Neese, F. The ORCA program system. *WIREs Comput. Mol. Sci.* **2012**, *2*, 73–78. [[CrossRef](#)]
42. Neese, F. Software update: The ORCA program system-Version 5.0. *WIREs Comput. Mol. Sci.* **2022**, *12*, e1606. [[CrossRef](#)]
43. Lu, T.; Chen, F. Multiwfn: A multifunctional wavefunction analyzer. *J. Comput. Chem.* **2012**, *33*, 580–592. [[CrossRef](#)]
44. Liu, Z.; Lu, T.; Chen, Q. An sp-hybridized all-carboatomic ring, cyclo[18]carbon: Electronic structure, electronic spectrum, and optical nonlinearity. *Carbon* **2020**, *165*, 461–467. [[CrossRef](#)]
45. Nyholm, R.S. Magnetochemistry: Introductory lecture. *J. Inorg. Nucl. Chem.* **1958**, *8*, 401–422. [[CrossRef](#)]
46. Bertini, I.; Luchinat, C. Relaxation. *Coord. Chem. Rev.* **1996**, *150*, 77–110. [[CrossRef](#)]
47. Nakamoto, K. *Infrared and Raman Spectra of Inorganic and Coordination Compounds*, 6th ed.; Wiley: Hoboken, NJ, USA, 2009.
48. Alvarez, S.; Avnir, D.; Llunell, M.; Pinsk, M. Continuous symmetry maps and shape classification. The case of six-coordinated metal compounds. *New J. Chem.* **2002**, *26*, 996–1009. [[CrossRef](#)]
49. Llunell, M.; Casanova, D.; Cirera, J.; Alemany, P.; Alvarez, S. *SHAPE, v. 2.1*; Universitat de Barcelona and the Hebrew University of Jerusalem: Barcelona, Spain, 2013.
50. van Albada, G.A.; Nur, S.; Mutikainen, I.; Turpeinen, U.; Reedijk, J. Characterisation and structure determination of two mononuclear Cu(II)(ClO₄)₂ compounds with 2,2'-bipyridine-1,1'-dioxide. *J. Mol. Struct.* **2008**, *875*, 91–95. [[CrossRef](#)]
51. Hnatejko, Z.; Kwiatek, D.; Durkiewicz, G.; Kubicki, M.; Jastrazab, R.; Lis, S. Pyridine N-oxide complexes of Cu(II) ions with pseudohalides: Synthesis, structural and spectroscopic characterization. *Polyhedron* **2014**, *81*, 728–734. [[CrossRef](#)]
52. van Albada, G.A.; Mutikainen, I.; Turpeinen, U.; Reedijk, J. Crystal structure and spectroscopy of the high-spin compound: Tris-(2,2'-bipyridine-1,1'-dioxide)Iron(III) tris(perchlorate) bis(acetonitrile), [Fe(bpdo)₃](ClO₄)₃(CH₃CN)₂. *J. Chem. Cryst.* **2001**, *31*, 75–79. [[CrossRef](#)]
53. Al-Karaghoul, A.R.; Day, R.O.; Wood, J.S. Crystal Structure of Tetrakis(2,2'-bipyridine dioxide)lanthanum Perchlorate: An Example of Cubic Eight-Coordination. *Inorg. Chem.* **1978**, *17*, 3702–3706. [[CrossRef](#)]
54. Huskowska, E.; Turowska-Tyrk, I.; Legendziewicz, J.; Riehl, J.P. The structure and spectroscopy of lanthanide(III) complexes with 2,2'-bipyridine-1,1'-dioxide in solution and in the solid state: Effects of ionic size and solvent on photophysics, ligand structure and coordination. *New J. Chem.* **2002**, *26*, 1461–1467. [[CrossRef](#)]
55. Malta, O.L.; Legendziewicz, J.; Huskowska, E.; Turowska-Tyrk, I.; Albuquerque, R.Q.; de Mello Donega, C.; e Silva, F.R.G. Experimental and theoretical study of ligand field, 4f–4f intensities and emission quantum yield in the compound Eu(bpyO₂)₄(ClO₄)₃. *J. Alloys Compd.* **2001**, *323*, 654–660. [[CrossRef](#)]
56. Zakrzewski, J.J.; Chorazy, S.; Nakabayashi, K.; Ohkoshi, S.-i.; Sieklucka, B. Photoluminescent Lanthanide(III) Single-Molecule Magnets in Three-Dimensional Polycyanidocuprate(I)-Based Frameworks. *Chem. Eur. J.* **2019**, *25*, 11820–11825. [[CrossRef](#)]
57. Jin, J.-C.; Lin, Y.-P.; Lin, L.-F.; Xiao, C.; Song, Y.; Shen, N.-N.; Gong, L.-K.; Zhang, Z.-Z.; Du, K.-Z.; Huang, X.-Y. 2,2'-Bipyridyl-1,1'-dioxide based bismuth(III) bromide hybrids: Studies on crystal structure and luminescence. *CrystEngComm* **2021**, *23*, 3744–3752. [[CrossRef](#)]
58. Mautner, F.A.; Fischer, R.C.; Reichmann, K.; Gullett, E.; Ashkar, K.; Massoud, S.S. Synthesis and characterization of 1D and 2D cadmium(II)-2,2'-bipyridine-N,N'-dioxide coordination polymers bridged by pseudohalides. *J. Mol. Struct.* **2019**, *1175*, 797–803. [[CrossRef](#)]
59. Sarma, R.; Boudalis, A.K.; Baruah, J.B. Aromatic N-oxide bridged copper(II) coordination polymers: Synthesis, characterization and magnetic properties. *Inorg. Chim. Acta* **2010**, *363*, 2279–2286. [[CrossRef](#)]
60. Kanno, H.; Omotera, Y.; Iijima, K. 2,2'-Bipyridine 1,1'-Dioxide. *Acta Crystallogr.* **1998**, *C54*, 149–151. [[CrossRef](#)]
61. Ye, M.-D.; Hu, M.-L.; Yuan, J.-X.; Wang, S. Crystal structure of 2,2'-bipyridine-1,1'-dioxide dihydrate, C₁₀H₈N₂O₂ · 2H₂O. *Z. Kristallogr. NCS* **2002**, *217*, 497–498. [[CrossRef](#)]
62. Luo, J.; Yang, F.; Qiu, L.-J.; Wang, X.-X.; Liu, B.-S. Bis(2,2'-bipyridine N,N'-dioxide)bis(tricyanomethanido)manganese(II). *Acta Crystallogr.* **2009**, *E65*, m547–m548. [[CrossRef](#)]

63. Tang, Y.-Z.; Wang, X.-S.; Zhou, T.; Xiong, R.-G. A Novel 2D Manganese(II) Coordination Polymer Exhibiting Ferromagnetic Interaction. *Cryst. Growth Des.* **2006**, *6*, 11–13. [[CrossRef](#)]
64. Groom, C.R.; Bruno, I.J.; Lightfoot, M.P.; Ward, S.C. The Cambridge Structural Database. *Acta Crystallogr.* **2016**, *B72*, 171–179. [[CrossRef](#)]
65. Qin, Y.; She, P.; Huang, X.; Huang, W.; Zhao, Q. Luminescent manganese(II) complexes: Synthesis, properties and optoelectronic applications. *Coord. Chem. Rev.* **2020**, *416*, 213331. [[CrossRef](#)]
66. Tao, P.; Liu, S.-J.; Wong, W.-J. Phosphorescent manganese(II) complexes and their emerging applications. *Adv. Opt. Mater.* **2020**, *8*, 2000985. [[CrossRef](#)]

Disclaimer/Publisher’s Note: The statements, opinions and data contained in all publications are solely those of the individual author(s) and contributor(s) and not of MDPI and/or the editor(s). MDPI and/or the editor(s) disclaim responsibility for any injury to people or property resulting from any ideas, methods, instructions or products referred to in the content.